LiF Crystal Advantages in Parametric X-Ray (PXR) Production

B. Sones, Y. Danon, and R. Block

Mechanical, Aerospace and Nuclear Engineering Department, Rensselaer Polytechnic Institute, Troy, NY 12180-3590, Sonesb@rpi.edu

INTRODUCTION

Parametric X-Rays (PXR) are derived from the interaction of relativistic electrons with the periodic structure of single crystals. PXR is an intense, polarized, and quasi-monochromatic x-ray production mechanism capable of providing tunable x-rays at angles well off of the electron beam direction. Because of its intensity and tunability, PXR has applications in medical imaging and material characterization [1].

PXR was first observed in 1985 at the Tomsk synchrotron when Baryshevsky, et al. [2] used 900 MeV electrons interacting with a diamond (220) crystal plane to produce 6.96 keV PXR. Since then, silicon has been the dominant choice for PXR characterization because of its structural stability and commercial availability [3]. Experimental PXR production using diamond, tungsten, and germanium were also reported [4,5,6,7,8].

TARGET MATERIALS TO MAXIMIZE PXR YIELD

The criterion for selecting the target material for an imaging application is to provide the greatest PXR photon yield with the least contamination of photons with other energies, termed here as noise. In ideal conditions, PXR photons are uniquely distributed about the Bragg condition with zero intensity at the Bragg angle [9]. The differential PXR yield is shown below.

$$\frac{d^2N}{d\theta_x d\theta_y} \propto f_{geo}\chi^2\left[\frac{\theta_x^{\,2}\cos^2 2\theta_B+\theta_y^{\,2}}{\sin^2\theta_B\left[\theta_x^{\,2}+\theta_y^{\,2}+\theta_{ph}^{\,2}\right]^2}\right]$$

The yield is dominated with three terms: the photon loss in the target material (f_{geo}), the electric susceptibility (χ), and, in large brackets, the shape of the photon distribution. Other variables are small angles θ_x (in the diffraction plane) and θ_y (perpendicular to the diffraction plane) relative to the Bragg condition with Bragg angle θ_B. The characteristic angle, θ_{ph}, defines the spread of the distribution. The first two terms compete. As PXR energy increases, the geometric term increases while the susceptibility decreases. A theoretical study of PXR yield integrated over a 1 mm^2 surface at 1 m from the crystal and at various detector angles is shown in Figure 1. This study included two materials, graphite and LiF, that are common in X-ray optics, but relatively overlooked in PXR production. The graphite and LiF PXR yields are high because of their minimal PXR absorption, while the Cu and W PXR yields are high because of their large electric susceptibilities.

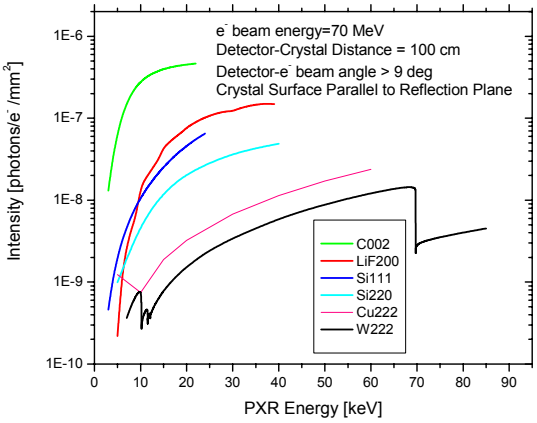

Fig. 1. Integrated PXR yield for LiF, graphite, Si, Cu, and W.

TARGET MATERIALS TO MAXIMIZE SIGNAL TO NOISE RATIO

The need to establish a clean environment in which to measure and use the produced PXR is as important as producing high PXR yield. Besides typical collimation and shielding, two related issues are important to consider: bremsstrahlung produced by the target crystal and detector dead time. At detector positions 20 degrees off the electron beam direction, MCNP [10] calculations predict that bremsstrahlung produced from Cu and W is at least an order of magnitude greater than from LiF. With this geometry, experiments using Cu (111) and W (222) resulted in signal to noise ratios at

unacceptable levels on the order of 0.003. A low Z material such as graphite provided more promising PXR signal to noise ratio of 0.4. This led to consideration of other low Z crystals like LiF. From Figure 1, LiF, Cu and W appear to be the most promising crystals for PXR energies greater than 25 keV. At 60 degrees off the electron direction (energies 12-14 keV), measured PXR yields from LiF (400), Cu (222), and W (222) were in agreement with calculated values with LiF, typically 4-5 times greater than Cu and W. For these experiments, all detected photons greater than 39 keV fell in last channel of the MCA. The fraction of primary PXR photons to photons greater than 39 keV was 1.44, 0.17, and 0.03 for LiF, Cu, W, respectively. Additional MCNP calculations suggest that the origin of most of these high energy photons is the target crystal itself [11].

LiF Compared with Graphite

From Figure 1, the choice of target crystals at energies less than 20 keV is clearly graphite or LiF. Since both are low Z targets, then the choice depends on the needed quality of PXR. While theory predicts that graphite will produce more PXR, the spectral purity of the PXR is degraded by the mosaic spread of graphite. For cubic crystals like LiF, orientation accuracy is effectively defined by the manufacturer polishing accuracy, typically 0.01 degree orientation accuracy. Mosaic spread of graphite inherently broadens the PXR energy distribution. Even with high purity oriented pyrolytic graphite (HPOG) with 0.4 degree mosaic spread, the PXR broadening effects are pronounced. Measurements of PXR production from LiF and graphite are shown in Figure 2. This figure demonstrates the increased photon production with graphite at the expense of a linewidth of 6.25%. By comparison, the energy linewidth for the LiF (400) crystal is 2.63% (330 eV), which is dominated by the detector resolution of ~270 eV.

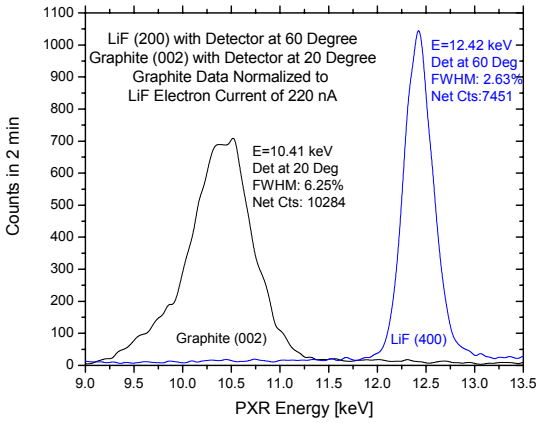

Fig. 2. Comparison of measured PXR yield and energy linewidth from LiF (200) and Graphite (002) with 0.4 degree mosaic spread.

RESULTS

In summary, we report for the first time production of parametric x-rays using a LiF target crystal. This crystal shows promise for its high PXR yield with relatively small bremsstrahlung production compared to other high yield, high Z crystals like Cu and W. As an alternative crystal with similar strengths, graphite has favorable PXR yield with low noise. However, because of its mosaic spread, graphite is less attractive than LiF for applications requiring nearly monochromatic x-rays and photon energy above 15 keV.

REFERENCES

1. M.A. Piestrup, X. Wu, V. V. Kaplan, S. R. Uglov, J. T. Cremer, D. W. Rule, R. B. Fiorito, *A design of mammography units using a quasimonochromatic x-ray source*, Rev. Scientific Inst. 72, 2159 (2001).

2. V.G. Baryshevshy, et. al., *Angular distribution of parametric X-rays*, Phys. Lett. 110A, 447 (1985).

3. F. Hagenbuck, et. al., *Novel Digital K-Edge Imaging System with Transition Radiation from an 855-MeV Electron Beam*, IEEE Transaction on Nuclear Science, Vol 48, No 3 (2001)

4. K.H. Brenzinger, et. al., *How narrow is the linewidth of parametric X-ray radiation?*, Phys. Rev. Lett. 79, 2462 (1997).

5. A.V. Shchagin, V.I. Pritupa, and N. A. Khizhnyak, *A fine structure of parametric X-ray*

radiation from relativistic electrons in a crystal, Phys. Let. A, 148, 485 (1990).

6. R. B. Fiorito, D. W. Rule, M. A. Piestrup, Qiang Li, A. H. Ho, and X.K. Maruyama, *Parametric X-ray generation from moderate energy electron beams*, Nuc. Inst. Methods B79, 758 (1993).

7. S. Asano, I. Endo, M. Harada, S. Ishii, T. Kobayashi, T. Nagata, M. Muto, K. Yashida, and H. Nitta, *How intense is parametric X radiation?*, Phys. Rev. Lett. 70, 3247 (1993).

8. T. Akimoto, M. Tamura, J. Ikeda, Y. Aoki, F. Fujita, K. Sato, A. Honma, T. Sawamura, M. Narita, and K. Imai, *Generation and use of parametric X-rays with an electron linear accelerator*, Nuc. Inst. Methods A459, 78 (2001).

9. Y. Danon,, B. Sones, R. Block, *Novel X-ray Source at the RPI LINAC*, Proceedings, ANS Annual Meeting, Hollywood, Florida, June 2002.

10. Monte Carlo N-Particle Transport Code (MCNP4C2), Los Alamos National Laboratory, Los Alamos, New Mexico, June 2001.

11. B. Sones, Y. Danon, R. Block, *Advances in Parametric X-Ray Production at the RPI Linear Accelerator*, Proceedings, ANS Annual Meeting, San Diego, California, June 2003.